Available online at www.sciencedirect.com
ScienceDirect
Polymer 48 (2007) 7632–7644
polymer
www.elsevier.com/locate/polymer

Comparison of polylactide/nano-sized calcium carbonate and polylactide/montmorillonite composites: Reinforcing effects and toughening mechanisms

Long Jiang, Jinwen Zhang*, Michael P. Wolcott

Wood Materials and Engineering Laboratory and Materials Science Program, Washington State University, P.O. Box 641806, Pullman, WA 99164, USA

Received 9 August 2007; received in revised form 23 October 2007; accepted 3 November 2007
Available online 7 November 2007

Abstract

Semicrystalline polylactide (PLA) exhibits high tensile strength and modulus but very low strain-at-break and toughness. In this study, PLA nanocomposites with nano-sized precipitated calcium carbonate (NPCC) and organically modified montmorillonite (MMT) clay were prepared by melt extrusion. Morphologies, tensile mechanical properties, dynamic mechanical and rheological properties, polymer–nanoparticle interactions, and toughening mechanisms of the PLA/NPCC and PLA/MMT nanocomposites were compared. MMT and NPCC showed significantly different effects on the strength, modulus and elongation of the PLA nanocomposites. Different toughening mechanisms were first elucidated for the two types of nanocomposites based on the evidence from both macroscopic and microscopic observations. Under uniaxial tension, large quantities of microvoids were created in both PLA nanocomposites. The microvoids in PLA/NPCC caused massive crazing, while in PLA/MMT they resulted in shear yielding, particularly in the nanocomposite with 2.5 wt% MMT. The MMT stacks and platelets were found to be located between the microvoids in the extended specimens and prevented them from collapsing and coalescing.

Keywords: Polylactic acid; Montmorillonite; Nanocomposites

1. Introduction

PLA offers a potential alternative to petrochemical plastics in many applications, in part because of its high strength and stiffness. However, its toughness, heat distortion temperature (HDT) and gas barrier properties are not satisfactory. Blending PLA with other polymers presents a practical and economic measure to obtain toughened products. To retain the integrity of biodegradability, blending PLA with other biodegradable polymers is particularly interesting. PLA/poly(ε-caprolactone) (PCL) blends have been extensively studied and have shown greatly improved mechanical properties compared to neat PLA [1–4]. In a recent study, we introduced PLA/poly(butylene adipate-*co*-terephthalate) (PBAT) blends and demonstrated a significant toughening effect [5]. In that study, we also first revealed the toughening mechanism of PLA with the PBAT inclusion.

Incorporating organically modified layered silicates (OMLS) into a PLA matrix has been studied extensively for improvements of HDT, dynamic mechanical, flexural, barrier properties, etc. [6–11]. In contrast, there are rarely published results on tensile and impact properties of PLA/OMLS nanocomposites, probably due to their poor performance compared to the pristine polymer. Nevertheless, two recent studies did report improved tensile properties of the PLA nanocomposites. Thellen et al. reported the increases in tensile strength, modulus and elongation of the blown film of PLA nanocomposites with 5 wt% montmorillonite [12]. Chang et al. also reported that the tensile strength and elongation of PLA nanocomposites with montmorillonite or synthetic mica at low nanofiller concentration (<4 wt%) were higher than those of neat PLA [13].

* Corresponding author. Tel.: +1 509 335 8723; fax: +1 509 335 5077.
E-mail addresses: jianglong@wsu.edu (L. Jiang), jwzhang@wsu.edu (J. Zhang), wolcott@wsu.edu (M.P. Wolcott).

0032-3861/$ - see front matter © 2007 Elsevier Ltd. All rights reserved.
doi:10.1016/j.polymer.2007.11.001

However, the micromechanical deformation process and toughening mechanism were not discussed in these studies. Even for other polymer/OMLS systems, many studies have reported increased Young's modulus but lowered tensile strength and strain-at-break or tensile toughness [14]. The increased tensile strength was discovered in the systems where strong polymer/OMLS interaction occurred [15–17]. The increases in both tensile strength and strain-at-break were only reported in elastomeric epoxy [18], polyurethane [19] and polyimide nanocomposites [20], but the toughening mechanism was not discussed.

If a good dispersion is achieved, rigid particle toughening will be more beneficial than rubber toughening since both stiffness and toughness can be increased by the former. It is our interest in this study to investigate the tensile properties and toughening mechanisms of PLA/nanoparticle composites. To better understand the reinforcing and toughening mechanisms, our approach is to compare the reinforcing and toughening effects of the MMT with those of NPCC, which possesses significantly different geometric structures and surface characteristics. The reinforcing effect of nano- and micro-sized $CaCO_3$ particles has been studied in polymer systems such as high density polyethylene (HDPE) [21], nylon [22], polypropylene (PP) [23], polyketone [24], acrylonitrile–butadiene–styrene (ABS) [25], and thermoplastic polyurethane (TPU) [26]. The tensile and/or impact toughness was found to be significantly improved by the addition of the fine $CaCO_3$ particles [21–24]. Large scale plastic deformation was found to be initiated by interfacial debonding and the subsequent relaxation of triaxial tensile stress [21–24].

To our knowledge, no studies on PLA/NPCC nanocomposites have been reported. Micromechanical deformation and toughening mechanisms of PLA nanocomposites have not been elucidated elsewhere. In this paper, we present the results of physical and mechanical properties of PLA nanocomposites with MMT and NPCC. The major aim of this study was to investigate the failure behavior and toughening mechanisms of PLA/MMT and PLA/NPCC nanocomposites under uniaxial tension. Reinforcing effects of the MMT and NPCC were studied and compared. Two different toughening mechanisms were identified for these two types of nanoparticles.

2. Experimental

2.1. Materials

Natureworks® PLA (4032D) was used and exhibited a weight-average molecular weight (M_w) of 207 kDa and polydispersity of 1.74 as determined by gel permeation chromatography. Differential scanning calorimeter (DSC) determined its glass transition temperature (T_g) and melting point (T_m) to be ca. 64 and 155 °C, respectively. The nano-sized precipitated calcium carbonate (NPCC201) was supplied by NanoMaterials Technology (Singapore). It was coated with stearic acid for better dispersion. The calcium carbonate particles are in cubic shape with an average primary particle size of ca. 40 nm. Its specific surface area is larger than 40 m^2/g (as per the manufacturer). Montmorillonite clay (I.34 TCN, Nanocor Inc.) was modified with methyl dihydroxylethyl hydrogenated tallow ammonium. The densities of NPCC, MMT and PLA were 2.55, 2.00 and 1.24 g/cm^3, respectively (data as per the manufacturers). The quaternary ammonium surfactant is derived from natural tallow, which contains a mixture of alkanes (C18/C16/C14 ratio: 0.66/0.31/0.03). It was reported to have a specific surface area of 750 m^2/g and a cation exchange capacity of 92 meq/100 g [27].

2.2. Nanocomposite preparation

A co-rotating twin-screw extruder (Leistritz ZSE-18) equipped with a volumetric feeder and a strand pelletizer was employed to compound PLA nanocomposites. The extruder had a screw diameter of 17.8 mm and an *L*/*D* ratio of 40. The extruder had eight controlled temperature zones which were set to range from 150 (next to the feeding segment) to 190 °C (die adaptor). The screw speed was maintained at 150 rpm for all runs. Before extrusion, PLA pellets, NPCC and MMT were dried at 90 °C in a convection oven for 12 h. The mixture of PLA and nanofillers was manually premixed by tumbling in a plastic zip-lock bag, and subsequently fed into the extruder for melt compounding. The extrudate was cooled in a water bath and subsequently granulated by a pelletizer. The PLA nanocomposites with 2.5, 5 and 7.5 wt% NPCC or MMT were prepared (1.2, 2.5, and 3.8 vol% for NPCC and 1.6, 3.2, and 4.8 vol% for MMT, respectively). Standard tensile (ASTM D638, Type I) test specimens were prepared by injection molding (Sumitomo SE 50D). Barrel temperatures were set at 170, 180, 190, and 190 °C from the feeding section to the nozzle, respectively. Mold temperature was 30 °C and cooling time was 30 s. Prior to injection molding, the pellets prepared from the extrusion were dried in a convection oven at 90 °C for 12 h.

2.3. Characterizations

The structures of the nanocomposites were evaluated by wide-angle X-ray diffraction (WAXD) (Siemens D-500) operating at 40 kV/20 mA with a Cu Kα radiation (wavelength, $\lambda = 0.154$ nm). The samples were scanned at 2 °C/min under the diffraction angle 2θ ranging from 2° to 30°. Fourier Transform Infrared Spectroscopy (FTIR) analysis was performed on film samples using a Thermo Nicolet Nexus 670 spectrometer. The spectra were recorded from 400 to 4000 cm^{-1} with a resolution of 2 cm^{-1} and 32 scans. Films of PLA and its nanocomposites were hot compressed from the injection molded plaques. Crystallization behavior of the composites was studied by differential scanning calorimetry (DSC) (Mettler Toledo, 822e) on the specimens sliced from injection molded samples. The specimens were crimp sealed in 40 μl aluminum crucibles. All specimens were kept isothermally at 180 °C for 3 min to erase previous thermal history. Then they were quenched to 20 °C at 50 °C/min and subsequently scanned from 20 to 180 °C at 5 °C/min. To investigate crystallinity gradient across the thickness of the injection molded composites,

samples sliced from the surface, intermediate, and core layers of the molded parts were scanned at the same rate without erasing their thermal history.

Dynamic mechanical properties of PLA and its composites were studied by dynamic mechanical analysis (DMA) (Rheometrics Solids Analyzer, RSAII). DMA specimens ($4 \times 2 \times 45$ mm^3) were cut from injection molded samples and tested using a dual-cantilever fixture at a frequency of 1 Hz. All tests were conducted at a strain of 0.04% using a 2 °C/min temperature ramp from 30 to 120 °C. Dynamic rheological properties of PLA and its composites were assessed using a strain-controlled rheometer (Rheometric Scientific, RDA III). Samples were tested using a parallel-plate geometry ($d = 25$ mm) operated at 180 °C. All samples were cut from the injection molded specimens. The gap distance between the parallel plates was 1 mm for all tests. A strain sweep test was initially conducted to determine the linear viscoelastic region of the materials. Dynamic frequency sweep tests (strain: 5%, frequency: 0.05 to 500 rad/s) were subsequently performed to determine the dynamic properties of the materials.

Tensile testing was performed on an 8.9-kN, screw-driven universal testing machine (Instron 4466) equipped with a 10-kN electronic load cell and mechanical grips. The tests were conducted at a crosshead speed of 5 mm/min with strains measured using a 25-mm extensiometer (MTS 634.12E-24). All tests were carried out according to the ASTM standard and 5 replicates were tested for each sample to obtain an average value. All samples were tested after one week of conditioning at 23 ± 2 °C and 50 ± 5% RH.

Fracture surfaces from tensile testing were examined using scanning electron microscopy (SEM) (Hitachi S-570). All specimens were sputter coated with gold prior to examination. The dispersion of NPCC and MMT in the PLA matrix was also assessed by transmission electron microscopy (TEM) (Jeol 1200 EX, accelerating voltage 100 kV). TEM ultrathin sections from the injection molded tensile samples were prepared by a Powertome X (Boeckeler Instrument) cryo-ultramicrotome. To study the micromechanical deformation and toughening mechanism of the nanocomposites, TEM sections were also cut along the tensile direction from the samples that had undergone tensile testing. The locations immediately below the fracture surfaces (sub-fracture region) were sectioned.

3. Results and discussion

3.1. Morphology of nanocomposites

WAXD reveals MMT gallery intercalation/exfoliation, while TEM can provide direct visualization of the structure, morphology, and spatial distribution of the various components in the nanocomposites. Fig. 1 shows WAXD patterns of the montmorillonite clay and its nanocomposites with PLA. The (001) and its higher order diffractions, e.g. (002) and (003), of the clay powder were registered at $2\theta \approx 2.96°$, 5.36° and 7.60°, respectively, which corresponded to a basal spacing of 2.98 nm, as well as 1.65 and 1.16 nm for the higher diffractions (lattice spacing d and diffraction angle θ is related

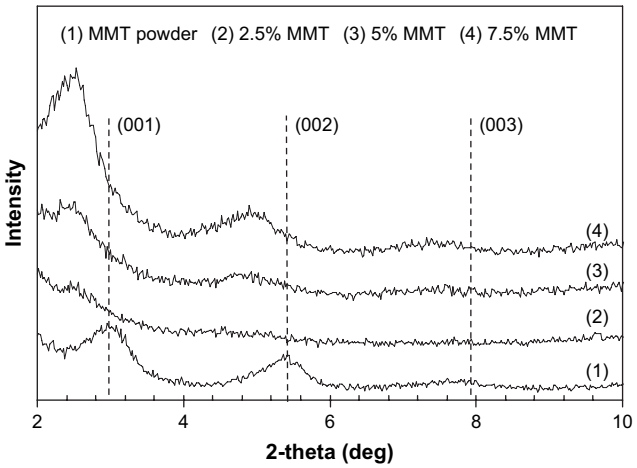

Fig. 1. WAXD patterns of PLA/MMT nanocomposites.

through Bragg's relation: $\lambda = 2d \sin\theta$, where λ is the wavelength of X-ray). In the nanocomposites, 2θ of the (001) diffraction was shifted to a lower angle ($\approx 2.54°$), with the corresponding gallery spacing enlarged to 3.47 nm. This indicates that the stacked layers of the MMT were intercalated by PLA chains. The spacings of the (002) and (003) planes were also increased to 1.79 nm ($2\theta \approx 4.94°$) and 1.17 nm ($2\theta \approx 7.52°$). The intensity of (001), (002) and (003) diffractions increased with the MMT content due to increased diffraction sites. The preservation of the three diffraction peaks in the nanocomposites indicates that a significant amount of MMT remained in layered form after the melt compounding process (although some might be exfoliated). As expected, NPCC and its nanocomposites with PLA showed no diffraction peaks at $2\theta < 10°$ (figure not shown), indicating the lack of ordered structure in the material.

Fig. 2 shows the dispersion of the MMT and NPCC in the PLA matrix. The dark fiber-like objects were stacks of MMT crystal platelets (Fig. 2a). Some stacks consisted of more platelets and appeared darker and thicker. The typical length and thickness of a fiber-like stack were ca. 200 and 5 nm, respectively. Given a platelet thickness of ca. 1 nm [28] and the measured gallery spacing of 3.47 nm, the thinnest stack consisted of a maximum of 2 layers of the crystal platelets. At high particle concentration (7.5 wt%), more agglomerates of MMT were visible in the composites (Fig. 2b) which could cause premature fracture in mechanical testing as discussed later in the tensile properties section. In Fig. 2c most NPCC were dispersed homogenously and existed in the PLA matrix as prime particles. They exhibited a cubic shape and measured ca. 30–40 nm in their largest dimension. Similar to MMT, at high particle concentration (7.5 wt%) more agglomerates of NPCC were also noted in the composites (Fig. 2d).

3.2. Interactions between PLA and nanoparticles

Fig. 3 presents the FTIR spectra of PLA and its nanocomposites. The peaks at 1027 and 3658 cm^{-1} were assigned to the C–O and O–H stretching of the $-CH(CH_3)-OH$ end group of PLA, respectively. Fig. 3 shows that neat PLA and

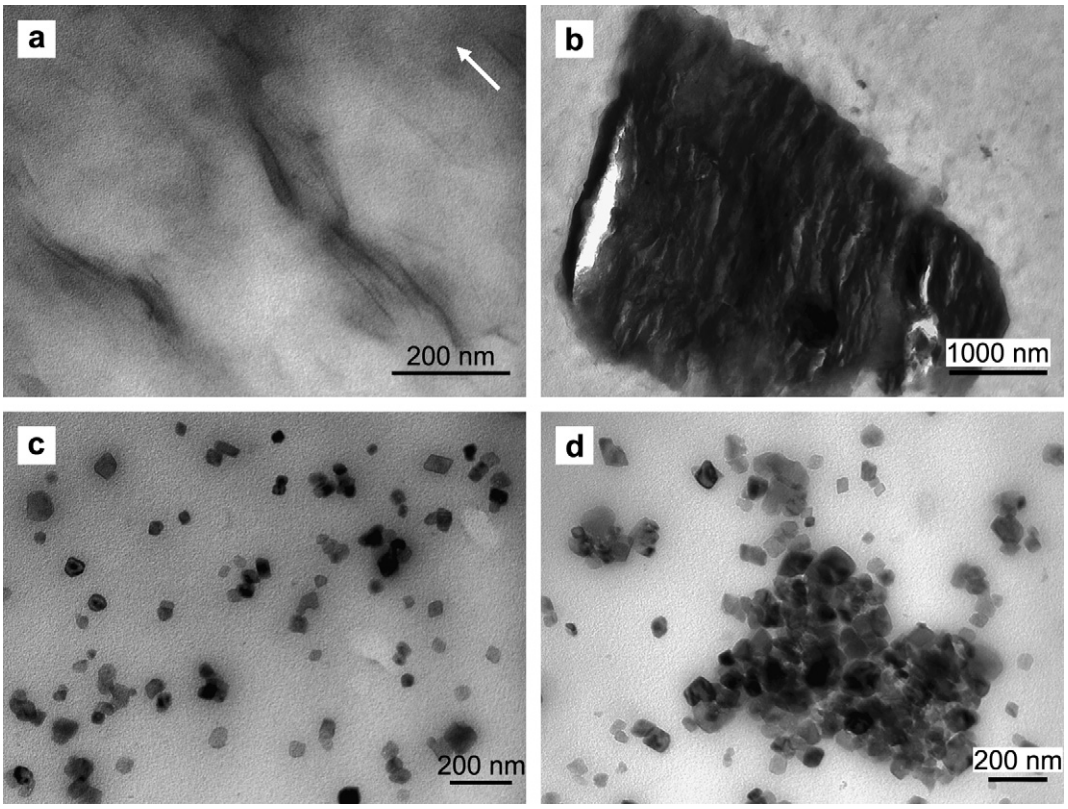

Fig. 2. TEM micrographs of PLA nanocomposites with MMT and NPCC: (a) 2.5 wt% MMT, (b) 7.5 wt% MMT, (c) 2.5 wt% NPCC and (d) 7.5 wt% NPCC. Arrow indicates flow direction.

PLA/NPCC exhibit the identical absorption peaks, suggesting lack of strong interactions between PLA molecules and NPCC particles. The stearic acid coating on the NPCC particles might present a barrier for the direct contact between PLA and NPCC, resulting in a weak polymer–particle interaction. In PLA/MMT the C–O and O–H stretching peaks were shifted to lower wavenumbers (1012 and 3633 cm^{-1}, respectively). This was attributed to the strong interactions between the PLA hydroxyl end groups and the MMT platelet surfaces and/or the hydroxyl groups of the ammonium surfactant in the organically modified clay. The splitting of the C=O stretching at ca. 1750 cm^{-1} might be due to the existence of urethane (–NH–CO–O–) groups, which was introduced by chain extension reaction. The high molecular weight of the PLA used in this study hinted that a diisocyanate chain extender was likely used in this commercial PLA resin.

3.3. MMT percolation network

Dynamic rheological testing reveals information about polymer chain structure and dynamics. G' of the composites with different particulate loadings are compared in Fig. 4. A homopolymer with narrow molecular weight distribution usually shows a characteristic terminal behavior of $G' \propto \omega^2$. Neat

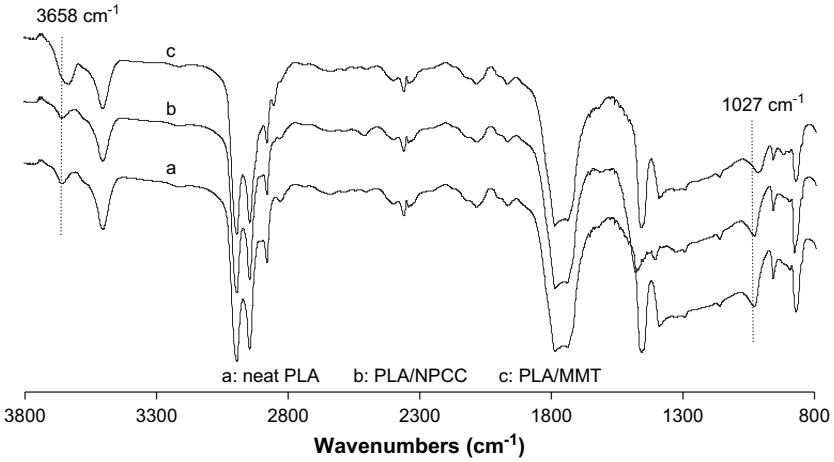

Fig. 3. FTIR spectra of neat PLA, PLA/NPCC and PLA/MMT.

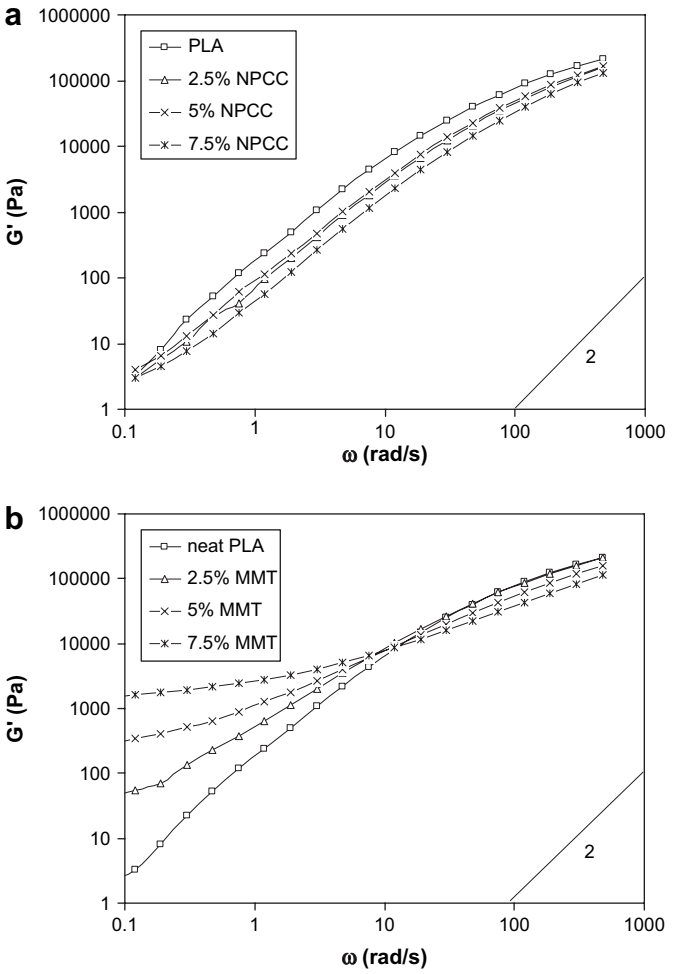

Fig. 4. G' of (a) PLA/NPCC and (b) PLA/MMT composites.

PLA followed this behavior fairly well ($G' \propto \omega^{1.9}$). The addition of NPCC did not change the shape and slope of the G' curves (Fig. 4a), indicating unaltered chain dynamics. On the other hand, G' of MMT filled PLA significantly deviated from the standard terminal behavior, from $G' \propto \omega^{1.1}$ for 2.5% clay to $G' \propto \omega^{0.1}$ for 7.5% clay (Fig. 4b). G' was nearly frequency-independent at high clay concentrations (>2.5 wt%), indicating a solid-like viscoelastic behavior. The pseudo-solid-like behavior indicates the formation of a MMT percolation network in the melt, in which a complete relaxation was prevented due to physical jamming [29]. MMT stacked layers (*i.e.* tactoids) exhibited local correlations and were incapable of free rotation beyond a critical volume fraction (percolation threshold). Garboczi et al. predicted the percolation threshold as a function of the aspect ratio of the ellipsoids for randomly oriented ellipsoids of revolution [30]. With an average tactoid aspect ratio of 40 (estimated from TEM micrographs), the percolation threshold of MMT was calculated to be 1.8 vol%. This result shows that percolation networks exhibited in both 5 and 7.5 wt% PLA/MMT nanocomposites (volume fraction 3.2% and 4.8%, respectively). NPCC did not form this network because of its low aspect ratio (~1, resulting percolation threshold 28.5 vol%). G' values of PLA/MMT were also much higher than those of PLA/NPCC, again indicating a more elastic, solid-like property of PLA/MMT due to the existence of the network structure. The percolation network structure of MMT and the strong interactions between MMT and PLA molecules differentiated MMT greatly from NPCC in reinforcing and toughening PLA as revealed in later sections.

DMA testing studies chain motion at glassy/rubbery state of the polymer. As shown in Fig. 5a, E' of PLA/NPCC composites precipitated after reaching the glass transition temperature (T_g) of PLA. The stiffness of the composites was so low that no valid E' data was able to be registered when the temperature increased further. The stiffness of the composites increased when the temperature was above ca. 90 °C due to cold crystallization of PLA [5]. Comparing Fig. 5b with 5a, PLA/MMT composites still maintained relatively high E' in the temperature range where E' of PLA/NPCC was too low to be measured accurately. E' of PLA/MMT was also found to increase with clay concentration in this temperature range. Neat PLA lost most of its stiffness when the temperature was above T_g. The stiffness of PLA/MMT above T_g originated from the percolation network of MMT, where polymer chain movement was restricted by the network structure [8]. It

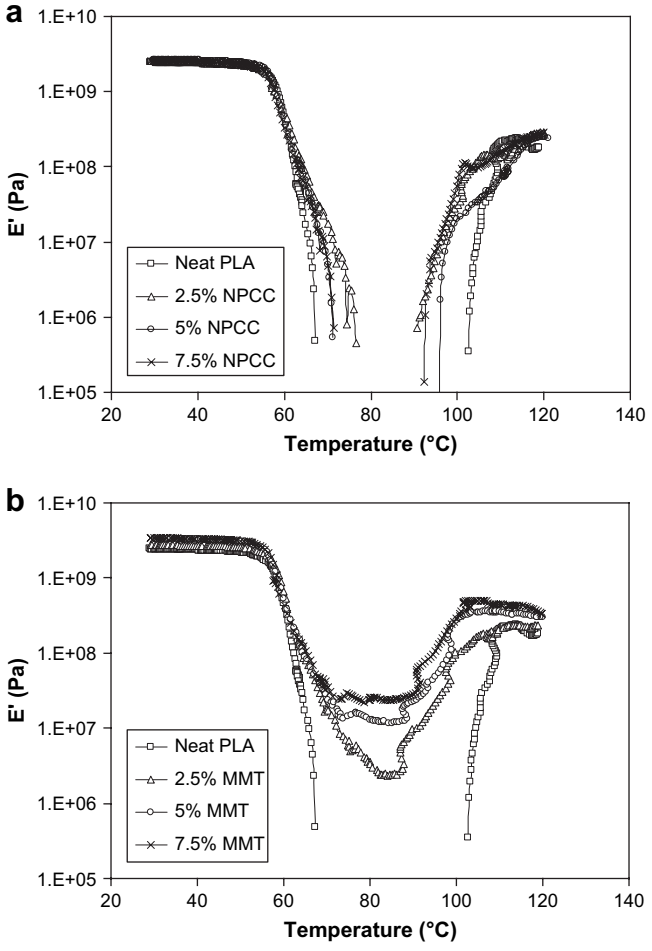

Fig. 5. Storage modulus of (a) PLA/NPCC and (b) PLA/MMT composites as a function of temperature.

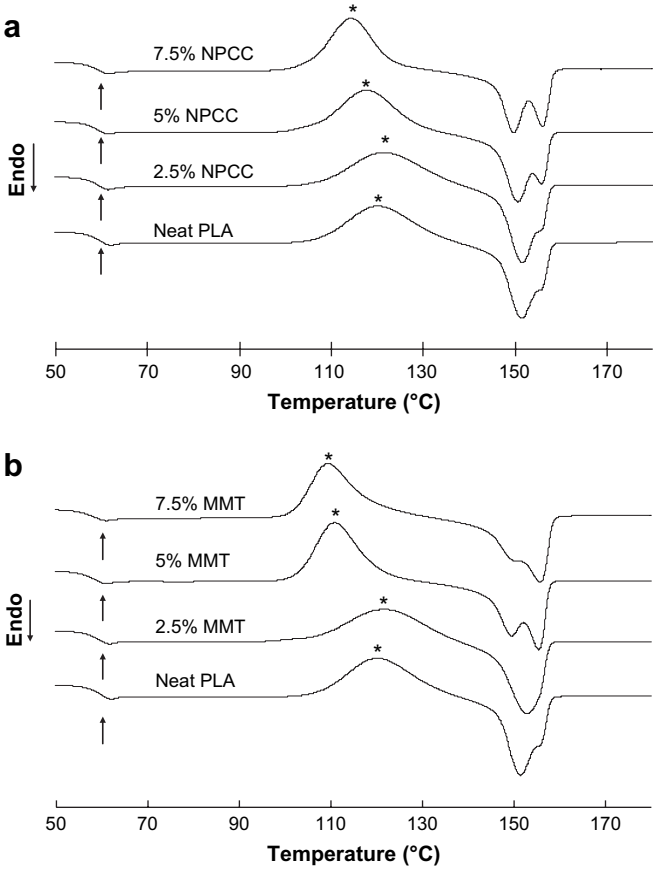

Fig. 6. DSC traces of (a) PLA/NPCC and (b) PLA/MMT composites at the heating rate of 5 °C/min. Data recorded from the samples quenched at 50 °C/min. (↑) Glass transition; (★) cold crystallization.

endowed the composites moderate stiffness/strength when the PLA matrix was in rubbery state at the raised temperatures.

3.4. Crystallization behavior

It is noted that some slowly crystallizing polymers, e.g. poly(phenylene sulfide) (PPS) and poly(ethylene naphthalate) (PEN) tend to form amorphous (skin)–semicrystalline (intermediate)–amorphous (core) type of multilayer structures in their injection molded parts [31,32]. This structural gradient is a combined result of thermal and stress crystallization [33]. To study the crystallinity gradient of the injection molded PLA nanocomposites, the crystallinity of the surface, middle and core layers of the molded part was monitored by DSC for up to seven days (conditioning time prior to mechanical testing) after the injection molding. The results indicated that samples from all 3 layers displayed strong PLA cold crystallization during DSC heating. The heat of cold crystallization was further found almost identical to the heat of fusion of the specimens (data not shown), suggesting that PLA did not crystallize at any part of the injection molded specimens. Therefore, the unique structural gradient occurring in some slowly crystallizing polymers did not appear in PLA nanocomposites. This was due to the combined effect of material crystallization ability and the injection molding conditions.

Because the mold temperature and cooling time were set at 30 °C and 30 s, PLA melt experienced a fast cooling process in injection molding. To understand the crystallization behaviors of the PLA nanocomposites, melt crystallization of PLA and its composites was studied by DSC using different cooling rates. No melt crystallization was observed even at the lowest cooling rate (10 °C/min, which is reasonably assumed to be much slower than the cooling in the injection molding). Pluta also obtained similar results on MMT filled PLA [34]. These findings confirm that PLA and its nanocomposites were amorphous when they were cooled down from the molten state.

Fig. 6 shows the DSC thermograms of PLA and composites in the second heat scan after fast cooling at 50 °C/min from the molten sate. The addition of NPCC or clay in PLA did not result in a noticeable change in the glass transition of PLA (ca. 64 °C). The cold crystallization temperature (120.6 °C) of the neat PLA was clearly decreased by the incorporation of NPCC and clay at 5 and 7.5 wt%, indicating an enhanced crystallization ability of PLA in the presence of nanofillers, which might behave as nucleating agents. At the same filler levels (5% and 7.5%), clay showed stronger nucleating effect than NPCC by giving a lower cold crystallization temperature (T_{cc}) and higher enthalpy of crystallization (ΔH_{cc}) (Table 1). This could be due to larger surface areas and volume ratios of the clay particulates, which gave rise to more nucleating sites. The very similar values of ΔH_{cc} and ΔH_m for each sample also indicated that the PLA was primarily amorphous.

In Fig. 6a, neat PLA shows a melting peak at 151.8 °C with a shoulder at 156.0 °C. The addition of an increasing amount of NPCC gradually decreased the size of the peak and transformed the shoulder into a second peak. This bimodal melting peak was induced during slow DSC scans when the less

Table 1
Characteristic thermal properties of PLA and its nanocomposites

Nanofiller ratio (%)	NPCC					MMT				
	T_{cc}[a] (°C)	ΔH_{cc}[b] (J/g)	T_m[a] (°C)		ΔH_m[b] (J/g)	T_{cc} (°C)	ΔH_{cc} (J/g)	T_m (°C)		ΔH_m (J/g)
			1	2				1	2	
0	120.6	23.4	151.8	156.0	23.5	120.6	23.4	151.8	156.0	23.5
2.5	122.1	27.4	151.9	155.9	26.9	122.2	25.9	152.7		26.6
5	118.3	28.6	150.9	156.2	29.0	110.8	30.0	149.5	155.4	30.0
7.5	115.0	30.2	149.9	156.4	30.4	109.4	31.1	150.3	155.7	31.0

T_{cc}: Cold crystallization temperature, ΔH_{cc}: enthalpy of cold crystallization, T_m: melting temperature and ΔH_m: enthalpy of fusion.
[a] T_{cc} and T_m are taken at the peak maximum of the crystallization and melting peaks.
[b] ΔH_{cc} and ΔH_m are corrected for the content of PLA in the blend.

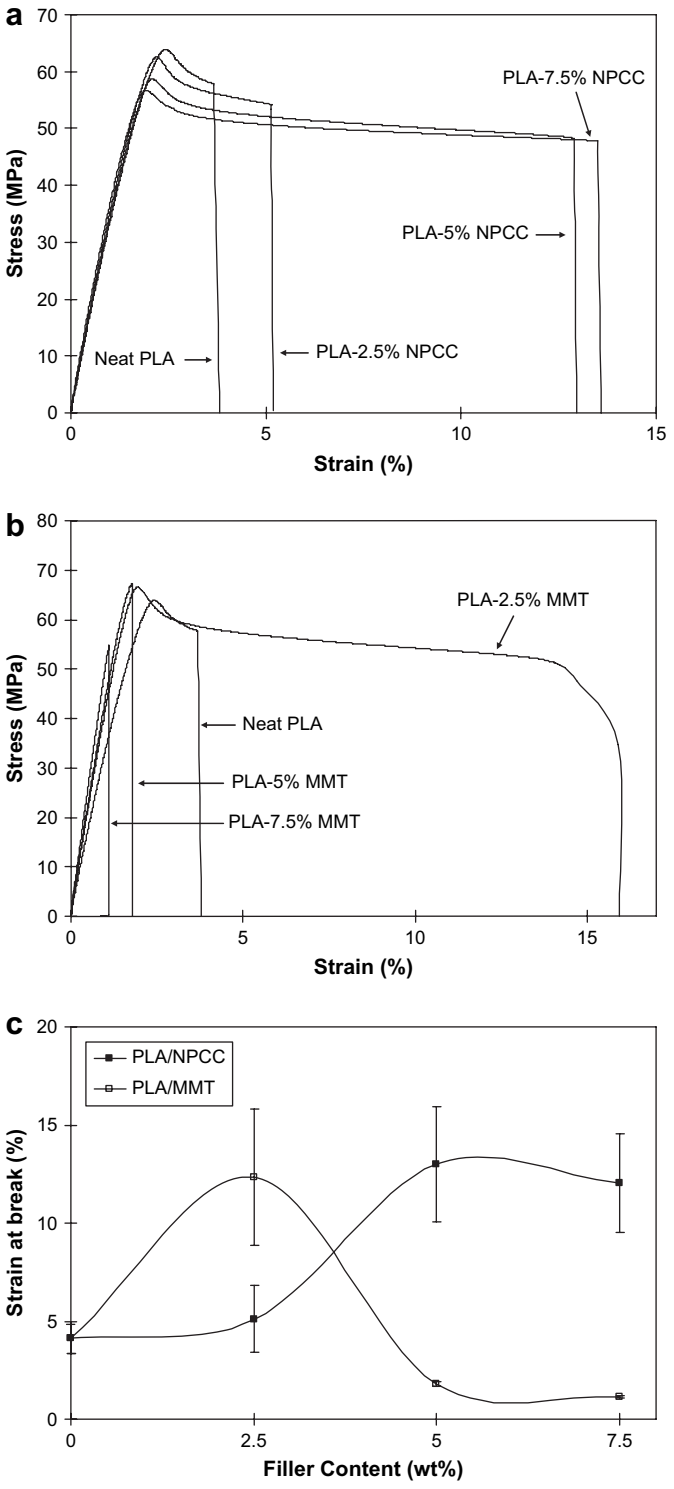

Fig. 7. Stress–strain curves of (a) PLA/NPCC, (b) PLA/MMT nanocomposites and (c) the comparison of their strain-at-break values.

perfect crystals had enough time to melt and reorganize into crystals with higher structural perfection, and remelt at higher temperature [35]. Low-temperature crystals have the same structure as the high-temperature ones, but with smaller lamellar thickness. The temperatures of the first peak decreased with the NPCC concentration, suggesting a larger number of less perfect crystals were nucleated at the particle surface. They reorganized into better form at higher temperature and melted again at about the same temperature. The same pattern of melting peak–shoulder transition happened in Fig. 6b, but at a faster pace. The peak in neat PLA was decreased to a shoulder in PLA-7.5% and the original shoulder was intensified to form a peak. In contrast to PLA/NPCC, the second melting peak of PLA/clay was larger than the first peak, implying the proportion of the less perfect crystals nucleated by the clay particulates was less than those nucleated by NPCC.

3.5. Tensile properties

Neat PLA exhibited yielding with a short quasi constant stress regime, and failed at ca. 4.1% strain (Fig. 7). The specimen yielded with stress-whitening bands (crazes) perpendicular to tensile direction all over the gauge length. All the neat PLA specimens fractured without necking. In the PLA/NPCC nanocomposites, the strain-at-break was increased to ca. 5.1% at 2.5 wt% NPCC, and ca. 13% at 5 and 7 wt% NPCC (Fig. 7a and c). All the PLA/NPCC nanocomposites yielded with noted stress whitening across the whole gauge length but without necking. Yield stress decreased with NPCC loading (Figs. 7a and 8) and was accompanied by more visually observable stress whitening in the specimen. On the other hand, Young's modulus showed a slight increase with NPCC. For the PLA/MMT nanocomposites, the addition of 2.5 wt% MMT resulted in a slight increase in yield stress (Figs. 7b and 8). The samples showed intense stress whitening followed by necking, resulting in a large yielding regime and hence significant strain-at-break (15.9%). With 5 and 7.5 wt% MMT, however, the strain-at-break was dramatically reduced to 1.8% and 1.1%, respectively, and the composite fractured in a completely brittle manner without yielding. Minor stress whitening was noted on 5 wt% composites and even less on 7 wt% composites. Young's modulus of the MMT nanocomposites significantly increased with MMT concentration. The strain-at-break (Fig. 7c) from different sample replicates exhibited a large variation. This was most likely because the failure strain was very sensitive to the condition of the specimen,

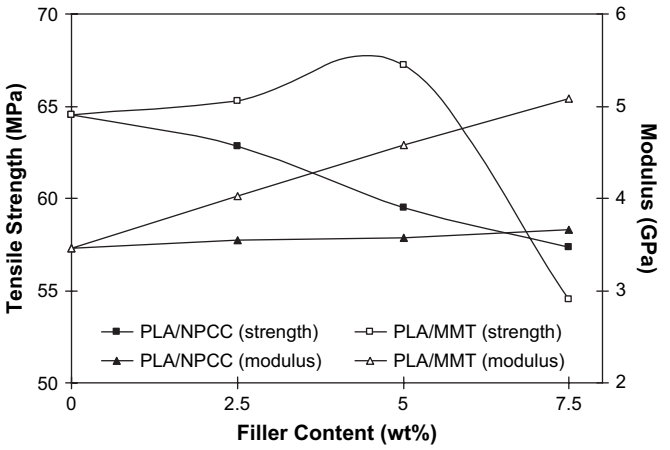

Fig. 8. Tensile yield strength and modulus of PLA/NPCC and PLA/MMT nanocomposites.

e.g., the dispersion of the inclusions, the presence of surface flaws, etc. The existence of large clusters of the inclusions triggered early brittle fracture of the material. In spite of the relatively large variations, the general trend of the strain-at-break as a function of filler content is still identifiable. These results clearly suggest that MMT and NPCC had different reinforcing and toughening effects on the PLA.

Massive crazing and shear yielding are two toughening mechanisms of polymers. For polymer toughening by rigid (non-deformable) particles, debonding at the particle surface can induce massive crazing, and/or shear yielding if the plastic resistance of the matrix is decreased to below the applied stress due to the release of strain constraints [36,37]. In a system where the interfacial adhesion is not high, debonding could occur at a lower tensile stress than the yield strength of the neat polymer [23]. This was the case for PLA/NPCC nanocomposites, where the tensile yield strength decreased with the NPCC content (Fig. 8) and strain-at-break increased by massive crazing. The relatively easy debonding of NPCC was probably attributed to two factors. First, the stearic acid coating on the particles limited the interactions between NPCC and PLA as revealed by FTIR. Second, the cubic-shaped NPCC particles caused a high stress concentration around the NPCC particles and promoted the debonding [37]. In contrast, addition of MMT at 5 wt% or lower enhanced the strength of PLA/MMT nanocomposites. The structure and surface characteristics of the MMT platelets were probably the main reason for the high strength and modulus of the MMT nanocomposites. With their large *L/D* ratio (ca. 40 from Fig. 2a), the MMT platelets induced lower stress concentration, which partly contributed to the higher strength of PLA/MMT compared to PLA/NPCC. The much larger surface area of the MMT (750 m^2/g compared to 40 m^2/g of NPCC) led to more interfacial area between the MMT and PLA. Moreover, PLA chains diffused into the tallow ammonium treated MMT gallery during melt compounding and established strong interaction with the tallow ammonium and the gallery surface, while the interaction between NPCC and PLA was limited due to the stearic acid coating. The large interfacial area and strong interfacial interaction increased stress transfer to the MMT platelets, resulting in high tensile strength of the PLA/MMT nanocomposites. According to micromechanical Halpin–Tsai theory, the much higher modulus of PLA/MMT compared to PLA/NPCC was a direct result of the MMT's high *L/D* ratio and its orientation along the tensile stress direction (flow direction) [38,39]. In terms of molecular dynamics, PLA chains were more restrained by the MMT platelets than the NPCC particles because of the former's larger interfacial area and stronger interaction. Global cooperative chain movement was suppressed by MMT tethering and gallery confinement [40–42]. Consequently, PLA/MMT showed a remarkably higher modulus than PLA/NPCC at the same filler ratio (Fig. 8).

The PLA/MMT nanocomposites (2.5 wt%) yielded at higher stress than the neat polymer and experienced significant necking. This suggested the occurrence of shear yielding. Above 2.5 wt% MMT, large aggregates of MMT particles might appear (Fig. 2b) and acted as material flaws, which triggered brittle response and early material failure in the tensile testing [22]. The debonding and subsequent shear yielding are further detailed in the next two sections.

3.6. Morphology of tensile fracture surfaces

The fracture surfaces after the tensile testing were studied by SEM. Polymer materials yield when crazing or shear yielding occurs. The fracture surface of crazing often appears more brittle than that of shear yielding in the sense that less plastic deformation can be detected on the fracture surface [43]. Neat PLA showed a fairly smooth fracture surface (Fig. 9a) due to the lack of large scale plastic deformation. A few fibrils can be seen which were formed during crazing. The fracture surfaces of PLA/NPCC showed more features because of larger plastic deformation caused by more crazes (Fig. 9b–d). On the fracture surface of PLA/2.5 wt% MMT nanocomposites which exhibited stress whitening and necking during tension, numerous fibrils were drawn out of the polymer, with cavities residing among them (Fig. 9e). The cavities were microvoids which initiated ligament shear yielding process during the tension. They could form at the polymer/MMT interface due to debonding or in the polymer matrix due to the microvoiding of the matrix. At 5 and 7.5 wt% MMT (Fig. 9f and g), the fracture surfaces were rough, with small cavities on the surface but no drawn-out fibrils, in agreement with their brittle fracture behavior. Fig. 9h and i shows two material flaws (*i.e.* large agglomerates of the filler, indicated by arrows) which initiated early fracture of the specimen.

3.7. Toughening mechanisms

To explore toughening mechanisms, tensile specimens were cryo-fractured longitudinally after the tension test and observed by SEM. Crazes were noted in the direction perpendicular to tensile stress on neat PLA and PLA/NPCC samples. Apparently these crazes were the consequences of those microvoids formed during tension, seen as stress whitening. Except for one craze (indicated by the arrow in Fig. 10a) in the area, neat PLA showed a smooth longitudinal surface without obvious plastic deformation. The addition of NPCC increased craze densities due to interfacial debonding at the polymer/NPCC interface (Fig. 10b–d). Crazing is a dilative process and involves localized plastic deformation [43]. Extensive crazing of the nanocomposites results in larger strain-at-break and higher toughness than those of neat PLA. It is also worth noting that aggregates of the NPCC are evident in all samples, which could cause early sample fracture and resulted in the large variation in strain-at-break values (Fig. 7c).

The 2.5 wt% MMT nanocomposite was the only PLA/MMT nanocomposite showing the necking behavior and a large strain-at-break value. Correspondingly, its SEM micrograph exhibited the most intensive plastic deformation (Fig. 10e), reflecting the large stretching of the ligament between the voids. At higher MMT concentrations (Fig. 10f and g), the surfaces were rough and grainy with MMT stacks

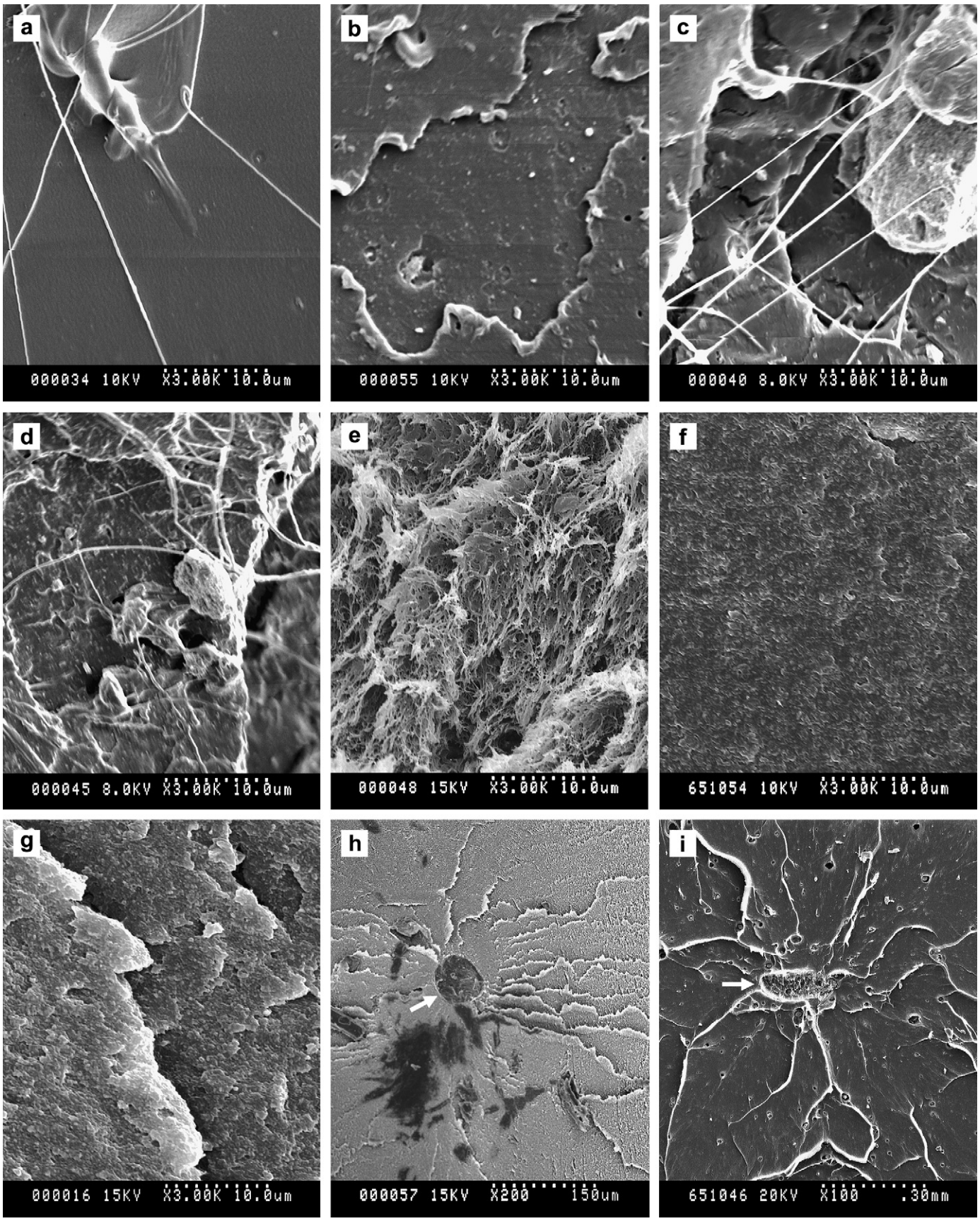

Fig. 9. SEM micrographs of the fracture surfaces of tensile specimens: (a) neat PLA, (b) 2.5 wt% NPCC, (c) 5 wt% NPCC, (d) 7.5 wt% NPCC, (e) 2.5 wt% MMT, (f) 5 wt% MMT, (g) 7.5 wt% MMT, (h) material flaw in 7.5 wt% MMT composite and (i) material flaw in 7.5 wt% NPCC composite.

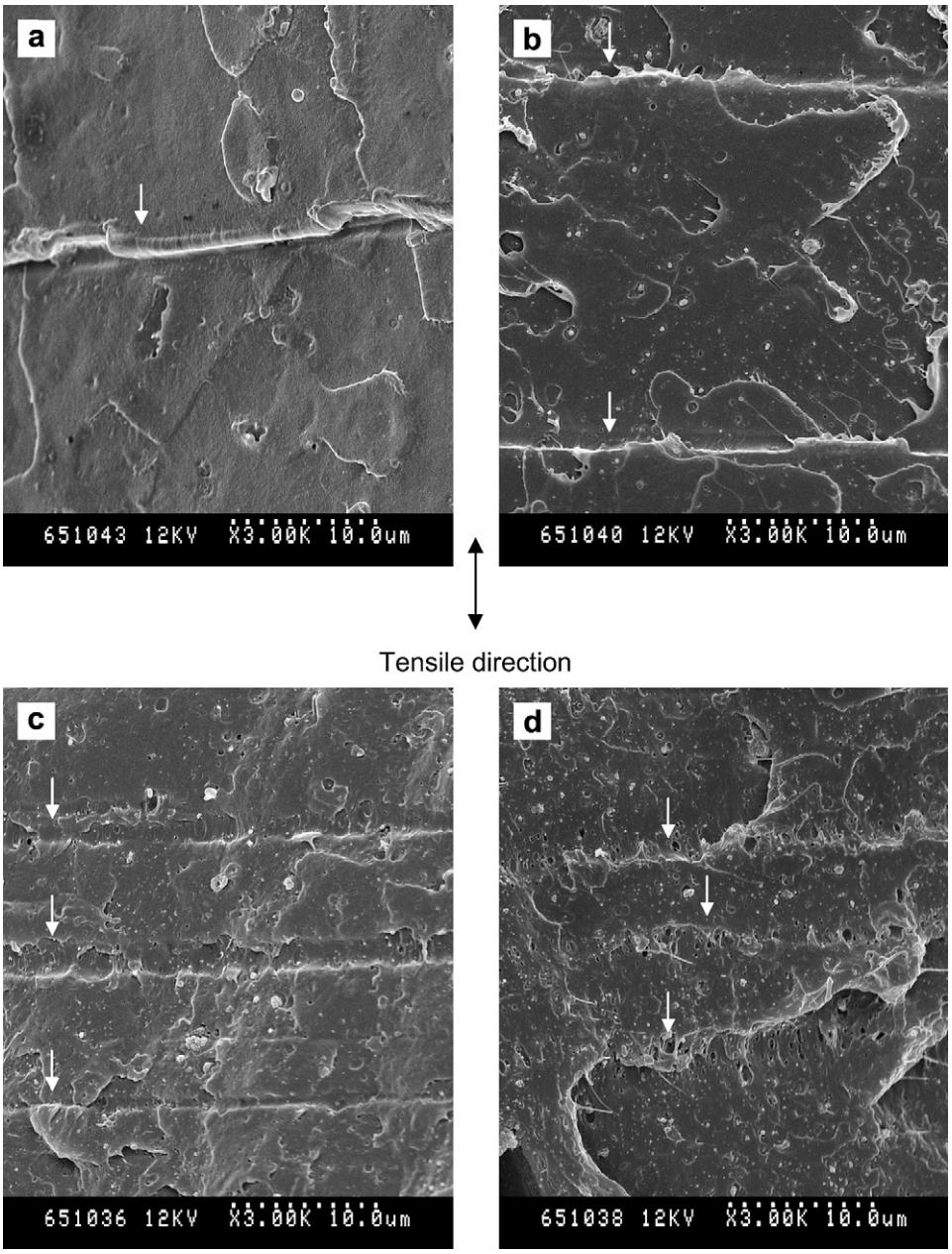

Fig. 10. SEM micrographs of the longitudinally cryo-fractured tensile specimens (a–g: after tensile testing. h: before tensile testing): (a) neat PLA, (b) 2.5 wt% NPCC, (c) 5 wt% NPCC, (d) 7.5 wt% NPCC, (e) 2.5 wt% MMT, (f) 5 wt% MMT, (g) 7.5 wt% MMT (inset is a micrograph at higher magnification) and (h) 7.5 wt% MMT before tension test.

embedded. Matching their brittle fracture behaviors (Fig. 9f and g), the morphological features of the plastic deformation were almost negligible in these two micrographs. Under higher magnification (Fig. 10g, inset), a small degree of plastic deformation along the tensile direction can still be seen between the MMT stacks (compared to Fig. 10h which shows the longitudinal surface before the tension test).

Micromechanical deformation of the tensile samples was further explored by TEM (Fig. 11). The formation of microvoids released strain constraints and induced local shear deformation in polymer ligaments. In this process, the MMT stacks may have performed dual roles: they provided microvoid nucleating sites at their surfaces so as to release the constraints for shear yielding, and to a large extent, they prevented the microvoids from coalescing and forming catastrophic cracks (Fig. 11a). The MMT stacks (indicated by the arrows in the photo) positioned between the elongated microvoids and formed a strong barrier preventing them from coalescing. Okamoto et al. found a similar structure in foamed MMT nanocomposites where the MMT aligned in the structs and enhanced mechanical properties of the composites [44]. When the MMT concentration was higher than 2.5 wt%, a MMT percolation network was formed as evidenced by rheological and DMA results. Cooperative chain motion was restrained by the network through the interaction between MMT and PLA chains. Hence, plastic deformation, which requires large scale

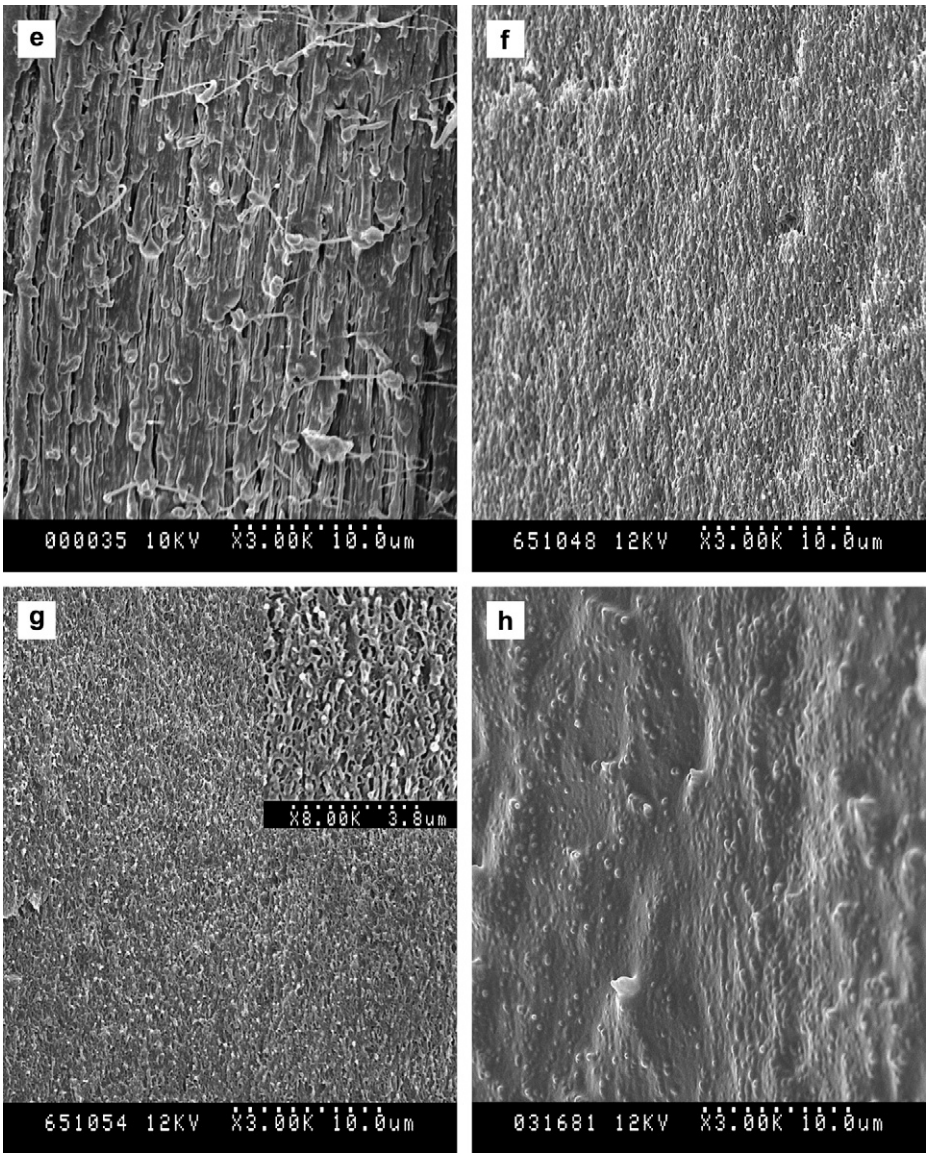

Fig. 10. (*continued*).

cooperative chain sliding and rotation, was more difficult to develop. Besides, high concentration of MMT led to more large agglomerates, which could trigger premature material failure (Fig. 11b). In PLA/NPCC nanocomposites, the formation of microvoids through debonding was evident (Fig. 11c). However, the cubic-shaped NPCC could not function in the same way as MMT to prevent the coalescence of the microvoids (Fig. 11d). These voids coalesced into cracks at the sites where the microvoids most densely located without inducing large scale shear deformation (Fig. 11e). Therefore, the subsequent necking could not be initiated.

It is worth mentioning that MMT platelets were found highly oriented along the flow direction in TEM micrographs. It has also been revealed that after injection molding nanocomposites filled with platelet-type nanofillers exhibit high order of chain orientation along the flow direction due to the shear amplification effect caused by the platelets [45–47]. This orientation state of both the platelets and the polymer chains played an important part in the higher strength and modulus of PLA/MMT nanocomposites than those of PLA/NPCC composites.

Based on the above evidence, we are able to draw conclusions on the toughening mechanisms and failure behaviors of the nanocomposites. Under uniaxial tension, neat PLA yielded due to microvoiding and the subsequent massive crazing of the polymer. The addition of NPCC particles promoted microvoiding through PLA/NPCC interfacial debonding. The coalescence of microvoids resulted in cracks and eventually led to material failure. No large scale plastic deformation was initiated due to the void coalescence. For PLA/2.5%-MMT nanocomposites under uniaxial tension, microvoiding occurred in the PLA matrix and at PLA/MMT interfaces. The large shear yielding of the ligaments was allowed to occur in this case because the MMT stacks and platelets formed strong barriers between microvoids, which prevented the void coalescence and propagation of the crazes.

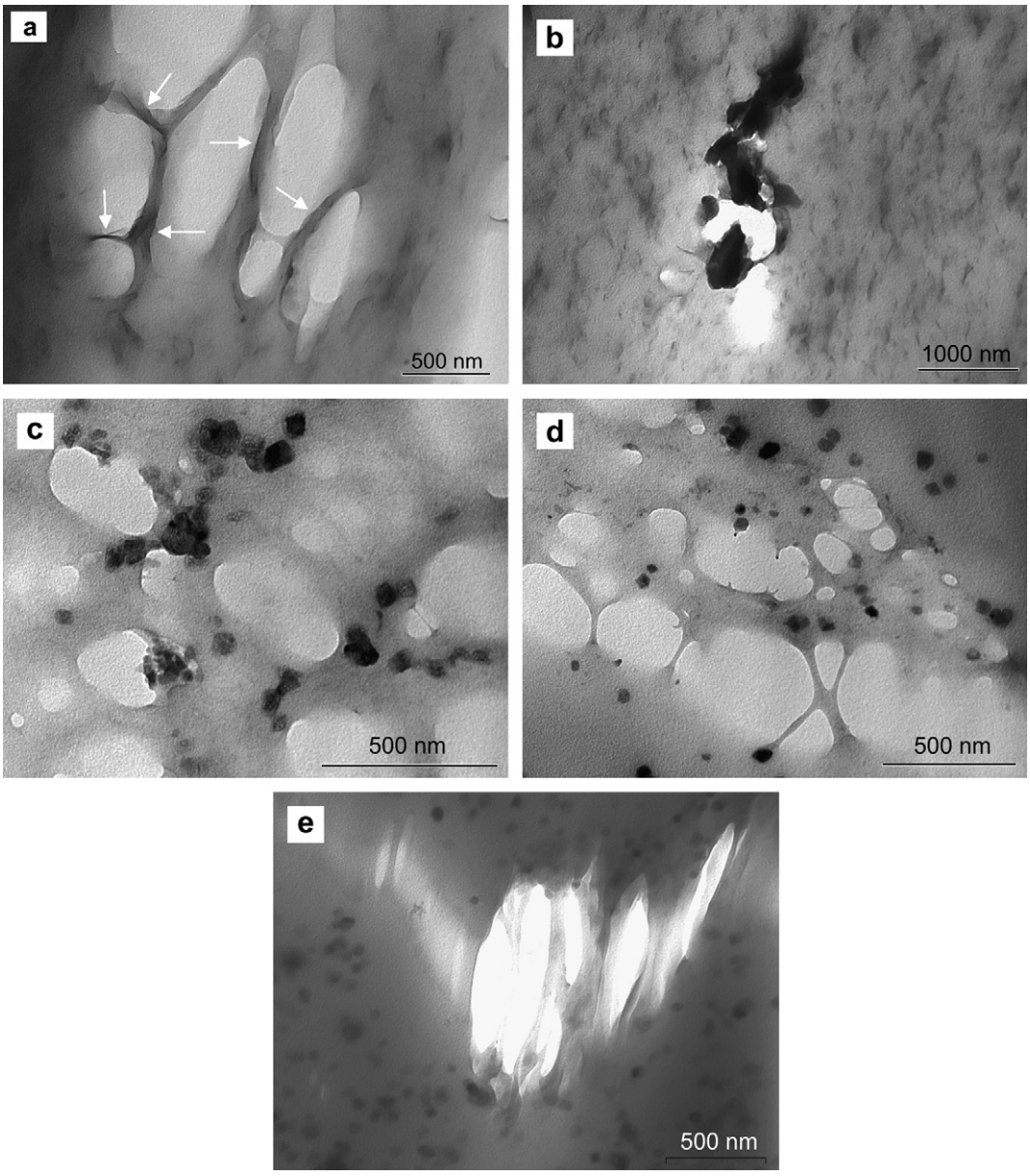

Fig. 11. (a and b) TEM micrographs of PLA/MMT and (c–e) PLA/NPCC nanocomposites showing microvoiding under uniaxial extension. TEM sections were cut from the sub-fracture parts of the samples that had undergone tensile testing. (a) 2.5 wt% MMT, (b) 7.5 wt% MMT and (c–e) 2.5 wt% NPCC.

4. Conclusions

PLA/NPCC and PLA/MMT nanocomposites were prepared by melt compounding using a twin-screw extruder and injection molded into test specimens. PLA in the injection molded specimens were found to be totally amorphous. Intercalation of MMT by PLA was revealed, and good dispersions of both nanoparticles were achieved when the filler concentration was $\leq$5 wt%. More large agglomerates were observed with increasing concentration of the filler. The strain-at-break of PLA increased with NPCC concentration ranging from 0 to 7.5 wt%, whereas it only increased with MMT concentration up to 2.5 wt% and decreased at higher concentrations. The tensile strength of PLA nanocomposites decreased with NPCC, whereas it increased with MMT up to 5 wt%. All PLA/NPCC nanocomposites showed clear stress yielding on the stress–strain curves but without noted necking. For PLA/MMT nanocomposites, stress yielding was only noted for the PLA/2.5 wt% MMT composite with significant necking. The different reinforcing effects of these two nanoparticles could be mainly attributed to the differences in microstructures and interactions between the nanoparticles and PLA in the respective nanocomposites. Evidence of micromechanical deformation from SEM and TEM micrographs suggested that NPCC increased the strain-at-break by massive crazing across the whole gauge length and the matrix eventually failed due to the coalescence of the microvoids. MMT at low concentration (e.g. 2.5 wt%) greatly increased the strain-at-break by shear yielding. Large scale shear deformation was found in the polymer ligaments between MMT stacks whereas such plastic shear deformation was absent in PLA/$CaCO_3$ nanocomposites. The MMT stacks located between the microvoids and

prevented their coalescence, allowing large scale shear yielding. At higher MMT concentrations, agglomerates induced premature material failure occurred before the shear yielding was able to start.

Acknowledgment

The authors are grateful to Ms. Amy Feng Chen and Mr. Bo Liu for their assistance in some of the experiments.

References

[1] Aslan S, Calandrelli L, Laurienzo P, Malinconico M, Migliaresi C. J Mater Sci Mater Med 2000;35:1615–22.
[2] Maglio G, Migliozzi A, Palumbo R, Immirzi B, Volpe MG. Macromol Rapid Commun 1999;20:236–8.
[3] Maglio G, Malinconico M, Migliozzi A, Groeninckx G. Macromol Chem Phys 2004;205:946–50.
[4] Kim CH, Cho KY, Choi EJ, Park JK. J Appl Polym Sci 2000;77:226–31.
[5] Jiang L, Wolcott MP, Zhang J. Biomacromolecules 2006;7:199–207.
[6] Sinha Ray S, Okamoto M. Prog Polym Sci 2003;28:1539–641.
[7] Sinha Ray S, Yamada K, Okamoto M, Ogami A, Ueda K. Chem Mater 2003;15:1456–65.
[8] Sinha Ray S, Maiti P, Okamoto M, Yamada K, Ueda K. Macromolecules 2002;35:3104–10.
[9] Chang JH, Uk-An Y, Sur GS. J Polym Sci Part B Polym Phys 2003;41:94–103.
[10] Maiti P, Yamada K, Okamoto M, Ueda K, Okamoto K. Chem Mater 2002;14:4654–61.
[11] Krikorian V, Pochan D. Chem Mater 2003;15:4317–24.
[12] Thellen C, Orroth C, Froio D, Ziegler D, Lucciarini J, Farrell R, et al. Polymer 2005;46:11716–27.
[13] Chang JH, An YU, Cho D, Giannelis EP. Polymer 2003;44:3715–20.
[14] Alexandre M, Dubois P. Mater Sci Eng R Rep 2000;28:1–63.
[15] Kojima Y, Usuki A, Kawasumi M, Okada A, Fukushima Y, Kurauchi T, et al. J Mater Res 1993;8:1185–9.
[16] Fornes TD, Yoon PJ, Keskkula H, Paul DR. Polymer 2001;42:9929–40.
[17] Lan T, Pinnavaia TJ. Chem Mater 1994;6:2216–9.
[18] Wang Z, Pinnavaia TJ. Chem Mater 1998;10:1820–6.
[19] Wang Z, Pinnavaia TJ. Chem Mater 1998;10:3769–71.
[20] Yang Y, Zhu ZK, Yin J, Wang XY, Qi ZE. Polymer 1999;40:4407–14.
[21] Bartczak Z, Argon AS, Cohen RE, Weinberg M. Polymer 1999;40:2347–65.
[22] Wilbrink MWJ, Argon AS, Cohen RE, Weinberg M. Polymer 2001;42:10155–81.
[23] Zuiderduin WCJ, Westzaan C, Huétink J, Gaymans RJ. Polymer 2002;44:261–75.
[24] Zuiderduin WCJ, Huétink J, Gaymans RJ. Polymer 2006;47:5880–7.
[25] Jiang L, Lam YC, Tam KC, Chua TH, Sim GW, Ang LS. Polymer 2005;46:243–52.
[26] Jiang L, Lam YC, Tam KC, Li DT, Zhang J. Polym Bull 2006;57:575–86.
[27] Shanmuganathan K, Razdan S, Dembsey N, Fan Q, Kim YK, Calvert PD, et al. Mater Res Soc Symp Proc 2006;887. 0887-Q02-01.1.
[28] Giannelis EP, Krishnamoorti R, Manias E. Adv Polym Sci 1999;118:108–47.
[29] Ren J, Silva AS, Krishnamoorti R. Macromolecules 2000;33:3739–46.
[30] Garboczi EJ, Snyder KA, Douglas JF, Thorpe MF. Phys Rev E 1995;52:819.
[31] Hsiung CM, Cakmak M, White JL. Int Polym Proc 1990;5:109.
[32] Ulcer Y, Cakmak M. Polymer 1994;35:5651.
[33] Ulcer Y, Cakmak M, Miao J, Hsiung CM. J Appl Polym Sci 1996;60:669–91.
[34] Pluta M. Polymer 2004;45:8239–51.
[35] Sarasua JR, Prud'homme RE, Wisniewski M, Borgne AL, Spassky N. Macromolecules 1998;31:3895–905.
[36] Kinloch AJ. Adv Polym Sci 1985;72:45–67.
[37] Argon AS, Cohen RE. Polymer 2003;44:6013–32.
[38] Halpin JC. Primer on composite materials analysis. Pennsylvania: Technomic; 1992.
[39] Fornes TD, Paul DR. Polymer 2003;44:4993–5013.
[40] Zax DB, Yang DK, Santos RA, Hegemann H, Giannelis EP, Manias EJ. Chem Phys 2000;112:2945–51.
[41] Anastasiadis SH, Karatasos K, Vlachos G, Manias E, Fiannelis EP. Phys Rev Lett 2000;84:915–8.
[42] Krishnamoorti R, Vaia RA, Fiannelis EP. Chem Mater 1996;8:1728–34.
[43] Anderson TL. Fracture mechanics. 2nd ed. Boca Raton: CRC Press; 1995. p. 34, 322.
[44] Okamoto M, Nam PH, Maiti P, Kotaka T, Nakayama T, Takada M, et al. Nano Lett 2001;1:503–5.
[45] Yalcin B, Cakmak M. Polymer 2004;45:2691–710.
[46] Konishi Y, Cakmak M. Polymer 2005;46:4811–26.
[47] Yalcin B, Valladares D, Cakmak M. Polymer 2003;44:6913–25.